Accepted Manuscript

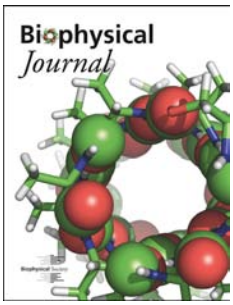

Enhancing biochemical resolution by hyper-dimensional imaging microscopy

Alessandro Esposito, Ashok R. Venkitaraman

PII: S0006-3495(19)30333-9

DOI: https://doi.org/10.1016/j.bpj.2019.04.015

Reference: BPJ 9657

To appear in: *Biophysical Journal*

Received Date: 25 January 2019

Accepted Date: 15 April 2019

Please cite this article as: Esposito A, Venkitaraman AR, Enhancing biochemical resolution by hyper-dimensional imaging microscopy, *Biophysical Journal* (2019), doi: https://doi.org/10.1016/j.bpj.2019.04.015.

Enhancing biochemical resolution by hyper-dimensional imaging microscopy

Alessandro Esposito[1,*] and Ashok R. Venkitaraman[1]

Running head: Hyper-dimensional imaging microscopy

Author affiliations:

[1]Medical Research Council Cancer Unit, University of Cambridge, Hills Road, Cambridge CB2 0XZ, UK

Correspondence:

Dr. Alessandro Esposito
MRC Cancer Unit, University of Cambridge
Hutchison/MRC Research Centre
Box 197, Biomedical Campus
Cambridge, United Kingdom
CB2 0XZ
+44(0)1223 330605 (office)
+44(0)1223 763241 (FAX)

Abstract

Two decades of fast-paced innovation have improved the spatial resolution of fluorescence microscopy to enable molecular resolution with low invasiveness and high specificity. Fluorescence microscopy also enables scientists and clinicians to map and quantitate the physico-chemical properties (e.g., analyte concentration, enzymatic activities and protein-protein interactions) of biological samples. But the biochemical resolving power of fluorescence microscopy is not as well-optimized as its spatial resolution. Current techniques typically observe only the individual properties of fluorescence, thus limiting the opportunities for sensing and multiplexing. Here, we demonstrate a new imaging paradigm — Hyper Dimensional Imaging Microscopy (HDIM) — that quantifies simultaneously and efficiently all the properties of fluorescence emission (excited state lifetime, polarization and spectra) in biological samples, transcending existing limitations. Such simultaneous detection of fluorescence features maximizes the biochemical resolving power of fluorescence microscopy, thereby providing the means to enhance sensing capabilities and enable heavily multiplexed assays. Just as multi-dimensional separation in mass-spectroscopy and multi-dimensional spectra in NMR have empowered proteomics and structural biology, we envisage that HDIM spectra of unprecedented dimensionality will catalyse advances in systems biology and medical diagnostics. **Introduction**

The biochemical environment of tissues and cells can be probed either by analysing the fluorescence of several naturally occurring, often metabolic-related, biomolecules (*e.g.*, various forms of nicotinamide adenine dinucleotide in its oxidised or reduced forms NAD^+/NADH) and flavin adenine dinucleotide (1, 2) or by analysing the fluorescence of environmentally sensitive fluorophores (*e.g.*, organic molecules and fluorescent proteins sensitive to pH) introduced into the sample by chemical or genetic means (3, 4). FRET (Foerster resonance energy transfer) is also a well-established and widely-used technique that enables cellular metabolism (*e.g.*, with glucose and ATP probes (5, 6)) and signalling (*e.g.*, with phosphorylation, acetylation and methylation probes (7)) to be mapped on single living cells. Often, these assays alter several properties of fluorescence. For instance, the heterogeneous biochemical milieu of tissues introduces complex optical-biochemical signatures into a specimen's fluorescence, or FRET alters spectra, lifetime and polarization of the FRET pair emission. However, state-of-the-art biochemical imaging techniques often rely just on the detection of simple optical features.

We hypothesized that the simultaneous detection of multiple characteristics of fluorescence would permit to extend significantly the biochemical resolving power in fluorescence microscopy, thus supporting more precise measurements or increased multiplexing capabilities *(e.g.*, multiple diagnostic markers or biochemical probes). Here, we illustrate the implementation of a novel detection paradigm that enables the parallel detection of all properties of fluorescence ("*hyper dimensional detection*", see **Supp. Text 1**) and provide the first analytical tools (*HDIM-toolbox*; see **Supp. Text 2**) to handle such complex datasets. We demonstrate how *Hyper Dimensional Imaging Microscopy* (HDIM) maximizes the biochemical resolving power of fluorescence microscopy and provide proof-of-concept experiments to illustrate how its increased resolution and multiplexed capabilities could be utilized in biomedical and clinical applications.

Materials and Methods

Microscopy and general principles of HDIM image analysis

Schematics of the microscope are shown in supporting information (**Fig. 1a** and **Figs. S2-S3**). Briefly, two photon excitation (TPE) is provided by a tunable femtosecond-pulsed Ti:Sapphire laser (Chameleon Vision 2, Coherent). TPE provides the ideal excitation for nanosecond lived excited state lifetime estimation, high dynamic range for anisotropy measurements (a maximum of 0.57 versus 0.4 for one photon excitation (8)) and permits the simple separation of the infrared excitation light from ultraviolet-visible fluorescence emission spectra and second harmonic signals. Care should be taken to avoid instabilities of the polarization of the excitation light. The system we developed was built around a Leica SP5 confocal/multi-photon microscope, which uses a periscope formed by a polarization beam splitter (PBS) and a mirror. The PBS works together with a half wave plate to finely tune the excitation power. The poor contrast ratio of a PBS and non-ideal performance of the reflection utilized in the periscope introduced elliptical polarization at the entrance of the microscope which we cleaned-up with a Glan-Thompson polarizer (Newport, see **Fig. S3**). HDIM detection was achieved by coupling two grating-based spectrographs (200nm bandwidth) with a polarizer beam splitter. Each spectrograph was equipped with a multi-anode photomultiplier tube and electronics for multi-dimensional time-correlated single photon counting. All TCSPC electronics, detectors and spectrographs were purchased from Becker&Hickl. Equipment for excitation, scanning and detection is commercially available; hardware and software for the integration of these parts have been developed in-house. The system design is described in **Figs. S2-S3** and can be easily replicated. The HDIM-toolbox is freely available at a GitHub repository (alesposito/HDIM-toolbox) and described in **Supplementary Methods**. At any given image pixel, this setup provides 16 spectral channels over 2 polarization states with arrival times typically histogrammed over 64 time bins. HDIM was calibrated with a laser comb provided by the standard laser lines of the confocal microscope (458nm, 488nm, 514nm, 561nm, 594nm, 633nm) back reflected by the objective lens and with a white light emitting diode which light was scattered by a frosted glass. Typical acquisition times for 256x256 pixels images were within the 1-2 minutes (solutions or *C. majalis* samples). Further details about sample preparation and imaging protocols can be found in **Supplementary Methods**. Images were acquired with a HCX PL APO CS 40x 1.25 NA oil objective with a 1.93 zoom thus imaging a field of view of 200µm side.

Sample preparation and analysis in solution

Fluorescent solutions were prepared from ethanol stock solutions of fluorescein (FITC, 1mM, Fluka Analytical) and rhodamine 6G (R6G, 5mM, Sigma-Aldrich) to a final concentration of 10µM and 1µM, respectevly. Aqueous solutions were prepared with 200µM KCl (Sigma-Aldrich) and a constant ethanol concentration (10% v/v). Fluorophores were quenched by equimolar substitution of KCl for Kl (100µM, Sigma-Aldrich) and their rotational correlation time increased with 65% v/v Glycerol (AnalaR NORMAPUR). The concentrations of the fluorophores were selected to provide a similar brightness with two-photon excitation at 840nm. We prepared twelve different solutions. Three solutions in 200µM KCl: FITC (F), R6G (R), FITC+R6G (D); in 100µM KCl and 100µM Kl: FITC (FQ), R6G (RQ), FITC+R6G (DQ); in 200µM KCl and Glycerol: FITC (FG), R6G (RG), FITC+R6G (DG); in 100µM KCl, 100µM Kl and Glycerol: FITC (FB), R6G (RB), FITC+R6G (DB). Solutions were imaged

sequentially in a glass-bottom microtiter plate. The characteristic spectra, fluorescence lifetimes and polarization anisotropies shown in **Fig. 1b-d** and in **Fig. S4** where shown after summing all photon-counts of the HDIM datasets along all the dimensions, but the spectroscopic dimension of interest. For example, one-dimensional spectra were computed by summing the HDIM images over the x, y, and pairs of time- polarization or spectral- bins. The distributions shown in **Fig. 1e-f** and **Fig. S5a-f** were obtained by summing the HDIM images along pairs of spectroscopic features as well, but not over space. A single spectral feature (spectral peak, average fluorescence lifetime and polarization anisotropy) was then evaluated in each pixel of the images and the resulting values were histogrammed to display the variability of the measurements, with the resulting distributions summed to create a single plot showing their relative separations. Principal component analysis (9) was performed on the full pixel ensemble of twelve HDIM datasets representative of the measured solutions after a 4x4 binning procedure in the x and y spatial dimensions for handling the large datasets. The trained PCA transform was then applied to the original full-size dataset independently and the distribution of individual components were then pooled together to show separations (**Fig. 1g**, **Fig. S4g-l** and **Fig. 2b**) as for the physical quantities (**Fig. 1e-f**, **Fig. 2a** and **Fig. S4a-f**) already described.

Sample preparation and analysis of C. majalis

C*onvallaria majalis* sections stained with Safranin and Fast Green, and mounted were purchased from Leica Microsystems UK (Cat. #As3211).

To provide digital images resembling counterstains used typically in histopathology (HE and DAB), we initially perform Principal Component Analysis on the pixel ensemble of an HDIM image. By definition, the principal component of PCA maximises contrast amongst the pixel hence providing a colour channel with the maximum contrast within the acquired image. The subsequent components provide a decreasing level of contrast until they contain just noise. The digital stains are generated with the function '*if_hdim_pca_rgb2dab*' included in the HDIM-toolbox. Briefly, each of the first four PCA component (n=1, 2, 3, 4) at each pixel location (i,j), was first stretched between the extreme values, $PCA(i,j)'_n = (PCA(i,j)_n - PCI^{min}_n)/(s(PCI^{max}_n - PCI^{min}_n))$. PCI^{min}_n is the minimum of each component within an image. However, aiming to moderate noise-dependent variations, PCI^{max}_n was computed empirically as the sum of the median of $PCA(i,j)_n$ with three standard deviations. *s* is a value computed to reach the desired level of saturation of the images which is optionally left equal to one or computed to re-stretch the $PCA(i,j)'_n$ values to saturate during the visualization at the 95% percentiles. All these operations are designed to achieve a good level of robustness in the automatic visualization of the stains. The colour projections are then computed on the resulting $PCA(i,j)'_n$ values. The HE-like representations (labelled as 'PCA>DAB3' by the HDIM-toolbox) visualize the first three PCA components as the magenta (M), cyan (C) and black (K) components of a CMYK image composite, where the yellow (Y) channel was left empty. The CMYK image composite was then projected to the red-green-blue (RGB) colour space for visualization. The DAB-like representation (labelled as 'PCA>DAB4' by the HDIM-toolbox) was computed in the same way but including the fourth (shown) or the sum of additional components (not shown) as the yellow channel of the CMYK composite before the colour transform to the RGB colour space. These transforms permitted to visualize the first three or four PCA components in colour spaces similar to histopathological counterstains.

Results

Improving biochemical resolving power

The formal description of the Fisher information for a multi-channel multi-parametric detection demonstrates the net increase in the biochemical resolving power that can be achieved theoretically (10). In **Fig. S1 and Supp. Text 2**, we provide a brief description of the theory and a simple graphical interpretation of the theoretical results. The '*photon partitioning theorem*' (10) predicts that the detection of photons into an increasing number of distinct "detection channels" tends to maximize information from the optical-biochemical system under investigation. Here, we test this prediction experimentally, with the engineering and testing of a detection system employing multiple parallel detection channels, each with electronics that generate histograms containing information about the polarization, colour and arrival time of each detected photon at every position within the sample.

Fig. 1a and **Figs. S2-S3** depict the experimental setup and the conceptual representation of HDIM. A pulsed laser (here a Ti:Sapphire laser for two-photon excitation) provides tightly controlled excitation light of known timing, polarization and spectra, which is delivered to the sample with a laser scanning microscope. Fluorophores and the biochemical environment of the sample reshape the excitation signal introducing complex optical signatures in the emitted fluorescence that are fully characterized by hyper-dimensional detection, achieved with a pair of multi-wavelength time-correlated single photon-counting detectors (see **Materials and Methods**). The photophysics (biochemistry) of the sample is thus described by 2,048 values, *i.e.* photon-counts accumulated into 16 spectral bins, 2 polarization states and 64 time-gates within each pixel of the acquired image. With the use of HDIM-tailored analysis algorithms, it is then possible to retrieve biochemical signatures from the complete photophysical characterization of the sample.

To demonstrate the sensing and un-mixing capabilities of HDIM, we imaged various solutions prepared with 1 µM rhodamine 6G and 10 µM fluorescein. Glycerol was used to reduce the rotational freedom of the fluorophores and equimolar substitution of potassium chloride with the quencher potassium iodide was employed to reduce their fluorescence lifetime (see **Figs. S4-S5** for the complete dataset). **Fig. 1b-d** shows how the emission spectra, lifetime and anisotropy of a mixture of rhodamine 6G and fluorescein are altered by their biochemical environment and how HDIM can sense these changes. By means of spectra of increasing dimensionality, HDIM can successfully separate different physico-chemical environments (**Fig. 1e-f**). **Fig. S5a-f** further demonstrates that the twelve different mixtures of rhodamine 6G, fluorescein, glycerol and potassium iodide can be resolved only with spectra of higher dimensionality compared to typical one-dimensional spectral information. We tested also the benefits of implementing Principal Component Analysis (PCA) as mean of contrast-enhancement for the analysis of HDIM datasets (see **Fig. 1g** and **Fig. S5g-l**). Three-dimensional spectra generated by photophysical features (**Fig. 2a**) or principal components (**Fig. 2b**) further illustrate the capability to increase the separability of different photophysical/biochemical features with spectra of higher dimensionality. To analyse the enhanced resolving power at increasing dimensionality, we quantified the separability (11) of different pixel-clusters with the Euclidian distance between their centroids divided by the root sum of their variance (**Fig. 2c-g**; see **Supplementary Methods**). The separability of pairs pixel-clusters might either improve or deteriorate with spectra of higher dimensionality. However, **Fig. 2** shows that the separability of the closest pixel-cluster (*i.e.*,

the worst resolved pair) improves at higher dimensionalities. It is possible to enumerate tens of different spectroscopic features (12) that could be extracted from an HDIM dataset aiming to improve the separability of these pixel-clusters. Instead, we have implemented principal component analysis to achieve a representation of the data that provide the smallest possible dimensionality together with the advantage of enhanced resolution provided by multi-dimensional datasets. **Fig. 2** shows that PCA can further improve the separability between different pixels. This is possible because PCA conveys all meaningful variation of spectra across different samples into the first components. Taken together, these experimental results and the underlying theory demonstrates that HDIM (multi-channel and multi-parametric imaging more generally) enhances the capability to sense and resolve differences in the photophysical/biochemical environment of the sample in fluorescence microscopy.

Contrast enhancement during post-processing

We then investigated whether the increased resolving power of HDIM could reveal structures – which would otherwise be invisible or poorly visible - when sensing individual optical properties. To test this possibility, we acquired images of *Convallaria majalis* stained with Safranin and Fast Green, a typical sample used to test microscopy techniques. **Fig. 3** illustrates the wealth of information that it is acquired by HDIM. In this case, the dataset is excitation-resolved as well by scanning the Ti:Sapphire laser from 750nm to 1000nm in steps of 50nm. We demonstrate how fluorescence lifetime, anisotropy and emission spectra change as function of excitation wavelength (**Fig. 3a**). The complexity of the optical signatures acquired by HDIM is shown in **Fig. 3b** as hyper-dimensional spectral signature or HDSS.

Fig. 4a shows an intensity image of the sample excited at 800nm. The specific optical properties of the sample can be mapped to two-dimensional maps through simple projections of the abstract 2,048-multidimensional space where each pixel can be described. Projections can be either based on physical quantities (*e.g.*, fluorescence anisotropy), statistical quantities (*e.g.*, PCA or non-negative matrix factorization) or perception-based features (*e.g.*, true colour). The latter is exemplified in **Fig. 4b** which is showing a red-green-blue (RGB) composite image of the specimen as if it was observed through the eyepieces by naked eye. To achieve this representation, first the 2,048-dimensional HDIM dataset is projected on a spectral-only space, effectively summing all photons in each individual time- and polarization- bins. Subsequently, photons from each spectral bin is weighted accordingly to an eye-sensitivity matrix and summed up into three colour channels. Similarly, representation of physical quantities can be synthesized by projecting the HDIM data on other dimensions without applying any weighing factor; for instance, **Fig. 4c,d** show synthetic fluorescence lifetime (FLIM) and anisotropy (FAIM) images (see also **Fig. S6**) generated by projecting HDIM datasets onto the relevant dimensions. To assess if the increased photophysical/biochemical resolution of HDIM translates into contrast enhancement (**Fig. 2b**), we also project the HDIM dataset to an RGB composite showing the first three principal components (**Fig. 4e-h** and **Fig. S6**). PCA is agnostic about the composition of the sample and it merely enhances the contrast for each and between each component. In fact, **Fig. 4e** shows structures of *Convallaria majalis* that colour, FLIM and FAIM images do not highlight. From the inspection of the individual principal components (**Fig. 4f-h**), it is possible to establish that Safranin and Fast Green are detected as first and

second principal components, respectively. Autofluorescence is loaded into the third principal component thus providing an additional mean of contrast.

Fig. 4i,j illustrates also how perception matrices can be exploited for possible future applications of HDIM to tissue diagnostics. Principal components can be projected to colour spaces resembling typical counterstains used in histopathology, such as hematoxylin and eosin (HE, **Fig. 4i,j** – left panels, two principal components) and in addition to 3,3′-Diaminobenzidine-like stain (DAB, **Fig. 4i,j** – right panels, three principal components). The full dataset from which **Fig. 4j** was computed is shown in **Fig. S6** (see also *HDIM-toolbox/if_hdim_pca_rgb2dab.m* in **Supplementary Files,** and **Materials and Methods**).

Taken together, these observations demonstrate that HDIM provides unprecedented sensing capabilities that can be exploited for contrast enhancement and to better resolve distinct biochemical/photophysical environments.

Discussion

Previously, we introduced a generalized concept of resolution in fluorescence microscopy, through which we demonstrated that from a theoretical perspective, it is possible to increase information content by increasing the number of independent detection channels, thus enhancing the sensing and unmixing capabilities of fluorescence microscopy (see the '*photon partitioning theorem*' and its corollaries in (10), **Fig. S1** and **Supp. Text 2**). From this theoretical foundation, we hypothesized that the simultaneous detection of orthogonal properties of light, such as fluorescence lifetime, polarization and spectra, could maximize the biochemical resolving power of fluorescence microscopy.

We report in this paper the results of work that provide proof-of-concept for this hypothesis. We introduce here a new detection paradigm (HDIM), wherein a time-resolved spectropolarimeter built with off-the-shelf components is utilized to fully resolve the fluorescence emission of specimens. We present here the first experimental evidence that HDIM can, in the first instance, provide unprecedented sensing capabilities. Rather than using filters or analysers to generate images during acquisition, HDIM datasets store the full spectroscopic information of a specimen resulting in datasets that can be projected onto spectral, lifetime and polarization dimensions during post-processing. We have also shown that projections can be performed not just on physical features but using statistical tools and perform perception-based projections. We envisage that HDIM will be particularly valuable when the optical signatures of a biological phenomenon are unknown - for instance, in tumour imaging, where HDIM sensing capabilities can be utilized as an artificial means of contrast enhancement.

Notably, our findings confirm that – as hypothesized – HDIM significantly enhances the resolving power in microscopy. HDIM exhibits spatial resolution equivalent to a laser scanning confocal or two-photon microscope; but in contrast, HDIM delivers enhanced resolving power to distinguish differences in photophysical properties. Therefore, HDIM can reveal structures that are photophysically distinct but that might be invisible to individual techniques (multi-colour or hyper-spectral imaging, fluorescence lifetime imaging and anisotropy imaging). Therefore, the capability to better resolve distinct emitters should also increase the capability to multiplex a larger number of fluorophores with known characteristics.

The analogy of a microscope as an information channel can be instructive to better understand the results we have presented here. When we prepare a fluorescence-based assay, we encode one or more random variables of interest *x* (*e.g.*, the concentration of analytes, rotational diffusions, or FRET efficiencies) into the spectroscopic features of the fluorophores. The transmitter (the light source and fluorophores) multiplexes information in the spectral-, time- and polarization- domains through the process of fluorescence. The hyper-dimensional spectral signature of a sample - *HDSS(x)* - changes smoothly with *x* and it is often highly correlated along different spectroscopic features. For instance, the change in relative abundance of two fluorophores exhibiting different fluorescence spectra, lifetime and anisotropy will result in a highly correlated change across the time- spectral- and polarization domains of the HDSS. The receiver (the optics, detectors and analysis algorithm) gather back information to reconstruct the message transmitted, *x*. By operating on the three orthogonal domains where information is spread, HDIM is an efficient receiver capable to demultiplex most of the available information, otherwise lost, and to retrieve a more precise representation of the original message (*x*).

We have previously described that the addition of 'detection channels' in fluorescence microscopy might result in practical disadvantages (10), *e.g.* increased read-out noise, optical losses or cost. However, efficient dispersive optics provide very high collection efficiencies (>80%, see for example (13)); single-photon counting provides high detection efficiencies limited only by intrinsic Poissonian noise of photon detection with virtually no read-out noise, and the typical speed limitations of photon-counting electronics are now overcome by recent developments (13-15). Furthermore, technologies currently beyond state-of-the-art, for instance, energy-resolving high-temperature superconducting single-photon detectors might provide efficient architectures for multi-parametric detectors also in fluorescence microscopy (16), in the future. Therefore, both with the elimination of technological barriers and by improving our understanding of information theory in fluorescence detection, we can significantly improve the resolving power of fluorescence microscopy, for the benefit of multiplexed sensing and biochemical imaging.

With faster and more cost-effective detection technologies being more readily available (13, 17-19), multiplexed detection technologies could be employed in a range of applications beyond the specialist laboratory. The advantages of multiparametric detection have been previously illustrated, ranging from applications in single-molecule spectroscopy (12) to fluorescence microscopy (20), including metabolic imaging (21, 22), quantification of interactions and molecular diffusion (23, 24) and tumour imaging (1, 25). A better understanding of a generalized concept of resolution in fluorescence microscopy and the implementation of technologies such as HDIM may thus impact several areas of biomedical relevance. By providing enhanced sensing and unmixing capabilities, HDIM may find utility, for instance, in contrast enhancement for label-free tissue imaging, in maximizing the multiplexing capabilities of diagnostic markers in histopathology or fluorescent probes in living cells (26). Furthermore, although we report here on imaging applications, hyper-dimensional detection can provide the same advantages when applied to spectroscopy or flow-cytometry. To empower the development of such applications, we have shared the software 'HDIM-toolbox', a toolbox that might facilitate the development of advanced analytical tools by the broader community. We suggest that heavily multiplexed imaging applications will synergize with emerging technologies such a smart-pixels and deep-

learning to significantly advance current capabilities for machine-vision and a broad range of biomedical applications.

Author contributions

AE designed and executed experiments, engineered the microscope and the analytical tools and analysed the data. ARV contributed to the critical analysis of the results. AE and ARV wrote the manuscript.

Acknowledgements

We acknowledge funding from the Medical Research Council core program grants (MC_UU_12022/1 and MC_UU_12022/8) awarded to ARV, and from the EPSRC grant (EP/F044011/1 and /2) to AE. We would like to thank Steve Scotcher, Howard Andrews, Phil Heard, Dave Cattermole and Martin Kyte from the mechanical and electronics workshop at the MRC LMB for their invaluable help with the engineering of our instrumentation. We also would like to thank Bryn Hardwick and Meredith Roberts-Thomson for the initial help with cloning, and Marina Popleteeva for discussion and support. We would like also to thank Leica Microsystems Ltd and Axel Bergmann at Becker&Hickl GmbH for their assistance in integrating electronics and microscopy tools. We acknowledge Prof. Hans Gerritsen (Utrecht University) for long and interesting discussions on the topic that led, among other things, to the definition of clearer nomenclature compared to that we used in early work.

References

1. Fereidouni, F., A. N. Bader, A. Colonna, and H. C. Gerritsen. 2014. Phasor analysis of multiphoton spectral images distinguishes autofluorescence components of in vivo human skin. J Biophotonics 7(8):589-596.
2. Trinh, A. L., H. Chen, Y. Chen, Y. Hu, Z. Li, E. R. Siegel, M. E. Linskey, P. H. Wang, M. A. Digman, and Y. H. Zhou. 2017. Tracking Functional Tumor Cell Subpopulations of Malignant Glioma by Phasor Fluorescence Lifetime Imaging Microscopy of NADH. Cancers (Basel) 9(12).
3. Miyawaki, A., J. Llopis, R. Heim, J. M. McCaffery, J. A. Adams, M. Ikura, and R. Y. Tsien. 1997. Fluorescent indicators for Ca2+ based on green fluorescent proteins and calmodulin. Nature 388(6645):882-887.
4. Kawanishi, T., L. M. Blank, A. T. Harootunian, M. T. Smith, and R. Y. Tsien. 1989. Ca2+ oscillations induced by hormonal stimulation of individual fura-2-loaded hepatocytes. The Journal of biological chemistry 264(22):12859-12866.
5. Kotera, I., T. Iwasaki, H. Imamura, H. Noji, and T. Nagai. 2010. Reversible dimerization of Aequorea victoria fluorescent proteins increases the dynamic range of FRET-based indicators. ACS Chem Biol 5(2):215-222.
6. Maioli, V., G. Chennell, H. Sparks, T. Lana, S. Kumar, D. Carling, A. Sardini, and C. Dunsby. 2016. Time-lapse 3-D measurements of a glucose biosensor in multicellular spheroids by light sheet fluorescence microscopy in commercial 96-well plates. Sci Rep 6:37777.
7. Rowland, C. E., C. W. Brown, I. L. Medintz, and J. B. Delehanty. 2015. Intracellular FRET-based probes: a review. Methods Appl Fluoresc 3(4):042006.
8. Volkmer, A., V. Subramaniam, D. J. Birch, and T. M. Jovin. 2000. One- and two-photon excited fluorescence lifetimes and anisotropy decays of green fluorescent proteins. Biophys J 78(3):1589-1598.
9. Le Marois, A., S. Labouesse, K. Suhling, and R. Heintzmann. 2017. Noise-Corrected Principal Component Analysis of fluorescence lifetime imaging data. Journal of Biophotonics 10(9):1124-1133.
10. Esposito, A., M. Popleteeva, and A. R. Venkitaraman. 2013. Maximizing the biochemical resolving power of fluorescence microscopy. PLoS One 8(10):e77392.
11. Kollner, M., and J. Wolfrum. 1992. How many photons are necessary for fluorescence-lifetime measurements. Chem. Phys. Lett. 200(1-2):199-204.
12. Prummer, M., B. Sick, A. Renn, and U. P. Wild. 2004. Multiparameter microscopy and spectroscopy for single-molecule analytics. Anal Chem 76(6):1633-1640.
13. Popleteeva, M., K. T. Haas, D. Stoppa, L. Pancheri, L. Gasparini, C. F. Kaminski, L. D. Cassidy, A. R. Venkitaraman, and A. Esposito. 2015. Fast and simple spectral FLIM for biochemical and medical imaging. Opt Express 18(23):23511-23525
14. Gersbach, M., R. Trimananda, Y. Maruyama, M. Fishburn, D. Stoppa, J. Richardson, R. Walker, R. K. Henderson, and E. Charbon. 2010. High frame-rate TCSPC-FLIM using a novel SPAD-based image sensor. P. Soc. Photo. Opt. Ins. 7780.
15. Krstajic, N., J. Levitt, S. Poland, S. Ameer-Beg, and R. Henderson. 2015. 256 x 2 SPAD line sensor for time resolved fluorescence spectroscopy. Opt. Express 23(5):5653-5669.
16. Natarajan, C. M., M. G. Tanner, and R. H. Hadfield. 2012. Superconducting nanowire single-photon detectors: physics and applications. Supercond Sci Tech 25(6):063001.
17. Esposito, A., H. C. Gerritsen, F. Lustenberger, T. Oggier, and F. S. Wouters. 2006. Innovating lifetime microscopy: a compact and simple tool for the life sciences, screening and diagnostics. J. Biomed. Opt. 11(3):034016.
18. Zhao, Q., B. Schelen, R. Schouten, R. van den Oever, R. Leenen, H. van Kuijk, I. Peters, F. Polderdijk, J. Bosiers, M. Raspe, K. Jalink, J. Geert Sander de Jong, B. van Geest, K. Stoop, and

I. T. Young. 2012. Modulated electron-multiplied fluorescence lifetime imaging microscope: all-solid-state camera for fluorescence lifetime imaging. J. Biomed. Opt. 17(12):126020.

19. Li, D. D. U., J. Arlt, D. Tyndall, R. Walker, J. Richardson, D. Stoppa, E. Charbon, and R. K. Henderson. 2011. Video-rate fluorescence lifetime imaging camera with CMOS single-photon avalanche diode arrays and high-speed imaging algorithm. J. Biomed. Opt. 16(9).
20. Bird, D. K., K. W. Eliceiri, C. H. Fan, and J. G. White. 2004. Simultaneous two-photon spectral and lifetime fluorescence microscopy. Appl. Optics 43(27):5173-5182.
21. Vishwasrao, H. D., A. A. Heikal, K. A. Kasischke, and W. W. Webb. 2005. Conformational dependence of intracellular NADH on metabolic state revealed by associated fluorescence anisotropy. The Journal of biological chemistry 280(26):25119-25126.
22. Yu, Q., and A. A. Heikal. 2009. Two-photon autofluorescence dynamics imaging reveals sensitivity of intracellular NADH concentration and conformation to cell physiology at the single-cell level. J Photochem Photobiol B 95(1):46-57.
23. Levitt, J. A., P. E. Morton, G. O. Fruhwirth, G. Santis, P. H. Chung, M. Parsons, and K. Suhling. 2015. Simultaneous FRAP, FLIM and FAIM for measurements of protein mobility and interaction in living cells. Biomed Opt Express 6(10):3842-3854.
24. Nguyen, T. A., P. Sarkar, J. V. Veetil, S. V. Koushik, and S. S. Vogel. 2012. Fluorescence polarization and fluctuation analysis monitors subunit proximity, stoichiometry, and protein complex hydrodynamics. PLoS One 7(5):e38209.
25. Fereidouni, F., K. Reitsma, and H. C. Gerritsen. 2013. High speed multispectral fluorescence lifetime imaging. Opt. Express 21(10):11769-11782.
26. Fries, M. W., K. T. Haas, S. Ber, J. Saganty, E. K. Richardson, A. R. Venkitaraman, and A. Esposito. 2018. Multiplexed biochemical imaging reveals caspase activation patterns underlying single cell fate. bioRxiv:427237.

Figure Captions

Figure 1 | Sensing and unmixing by hyper-dimensional imaging microscopy (HDIM). HDIM relies on the controlled excitation of the sample and by the analysis of biochemical signatures introduced into the photophysical properties of fluorophores within the sample (**a**). Sensing the biochemical environment of fluorophores (here R6G and FITC) can be achieved with the simultaneous detection of emission spectra (**b**), fluorescence lifetime (**c**) and anisotropy (**d**). Unmixing of different biochemical environment sensed by R6G and FITC is enhanced by the increased dimensionality of the analysed photophysical signatures: spectral peak (**e**), spectral peak *vs* lifetime (**f**) and by PCA (**g**). Peaks are marked with the labels "F" for FITC, "R" for R6G and "D" for a R6G and FITC mixture, followed by "0" (0% glycerol, 200 μM KCl), G (65% glycerol, 200 μM KCl), Q (0% glycerol, 100 μM KCl, 100 μM KCl) or B (65% glycerol, 100 μM KCl, 100μM KI). Red and orange labels indicate non-resolved and partially overlapping peaks, respectively. Excitation: 840nm.

Figure 2 | Improving biochemical resolving power by HDIM. We can build three-dimensional spectra utilizing physical properties of fluorescence (**a**, lifetime *vs* anisotropy *vs* wavelength) or principal components (**b**). Each multidimensional spectra (either 2D as in **Fig. 1**, **Fig. S5** or 3D in panel **a-b**) results in difference statistical confidence for separating the tested samples. Panel **c**) shows how 2D spectra of physical quantities provides good results, but with several peaks that are less resolved. The arrows indicate the worst performances for each type of analysis. **d**) Multivariate analysis improves significantly the confidence with which the closet objects can be separated; unsurprisingly, the first and second principal components (red arrow) provides the highest confidence. A direct comparison between PCA and physical quantities is shown for the three-dimensional spectra in panel **e**). The arrows indicate the worst performance of the two methods also in this representation. Panels **f** (blue: PCA spectra; red: Physical quantities; 1 to 3 indicates the pairs as per panels **c** and **d**, from top to bottom) and **g** plot the average separability index (S_{ij}) as defined in the **Supplementary Methods**.

Figure 3 | Sensing by hyper-dimensional imaging microscopy. Fluorescence lifetime decays (**a,** top-left), anisotropy spectra (**a**, top-center) and emission spectra (**a**, top-right) as a function of excitation wavelength measured on a single field of view of *Convallaria majalis*. The bottom panels show excitation-dependent distributions of fluorescence lifetimes (bottom-left) and anisotropies (bottom-right). Arrows and star highlight correlated features that are modulated by excitation wavelength. Example of hyper dimensional spectral signature (HDSS) at 800nm excitation wavelength (**b**). Time-decays are shown for its spectral and polarization components. On the back projection of the 3D plot, polarization-dependent spectra and anisotropy spectrum are shown, with the dashed yellow line marking the maximum of fluorescence anisotropy of 0.57 that can be measured with TPE.

Figure 4 | Unmixing by hyper-dimensional imaging microscopy. Images of *Convallaria majalis,* shown as total photon counts (**a**), and projections of HDSS values as true colour representation (**b**), fluorescence lifetime map (**c**), and fluorescence anisotropy map (**d**). Multivariate analysis of HDSS by PCA across the image provide a high contrast RGB composite (**e**) obtained by the overlay of the first three principal components (**f-h**). Digital stains derived from PCA can be projected to a colour-space analogous to the HE and DAB counter-stainings used in histopathology: (**i**) a field of view used for training PCA and (**j**) an independent imaged recoloured with the same projection matrix. Scale bar: 40µm; excitation: 800nm.

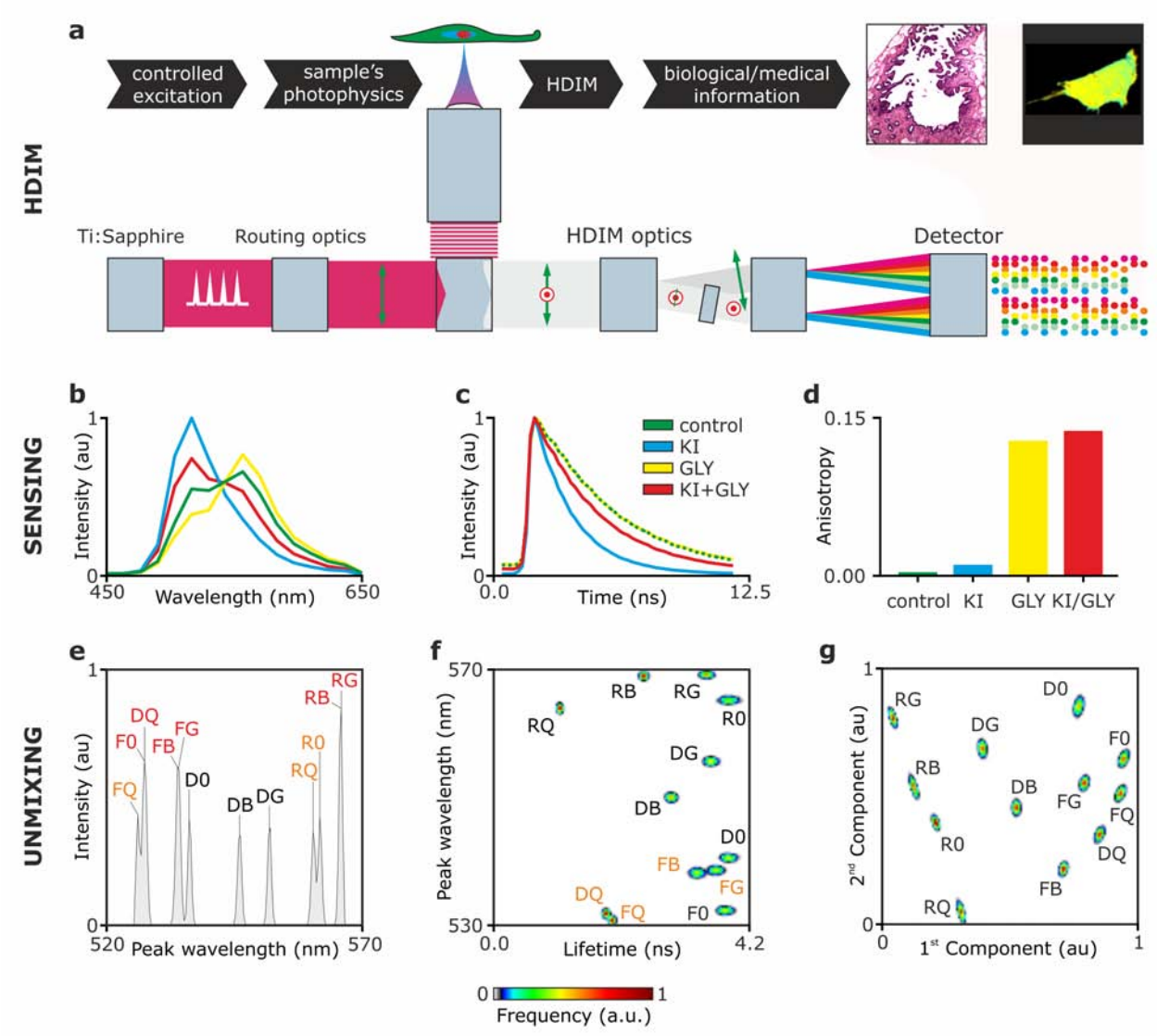
a
HDIM
controlled excitation
sample's photophysics
HDIM
biological/medical information
Ti:Sapphire
Routing optics
HDIM optics
Detector
SENSING
b
Intensity (au)
Wavelength (nm)
450
650
c
control
KI
GLY
KI+GLY
Time (ns)
12.5
d
Anisotropy
0.15
0.00
control
KI
GLY
KI/GLY
UNMIXING
e
Peak wavelength (nm)
520
570
f
Peak wavelength (nm)
Lifetime (ns)
4.2
Frequency (a.u.)
g
1st Component (au)
2nd Component (au)

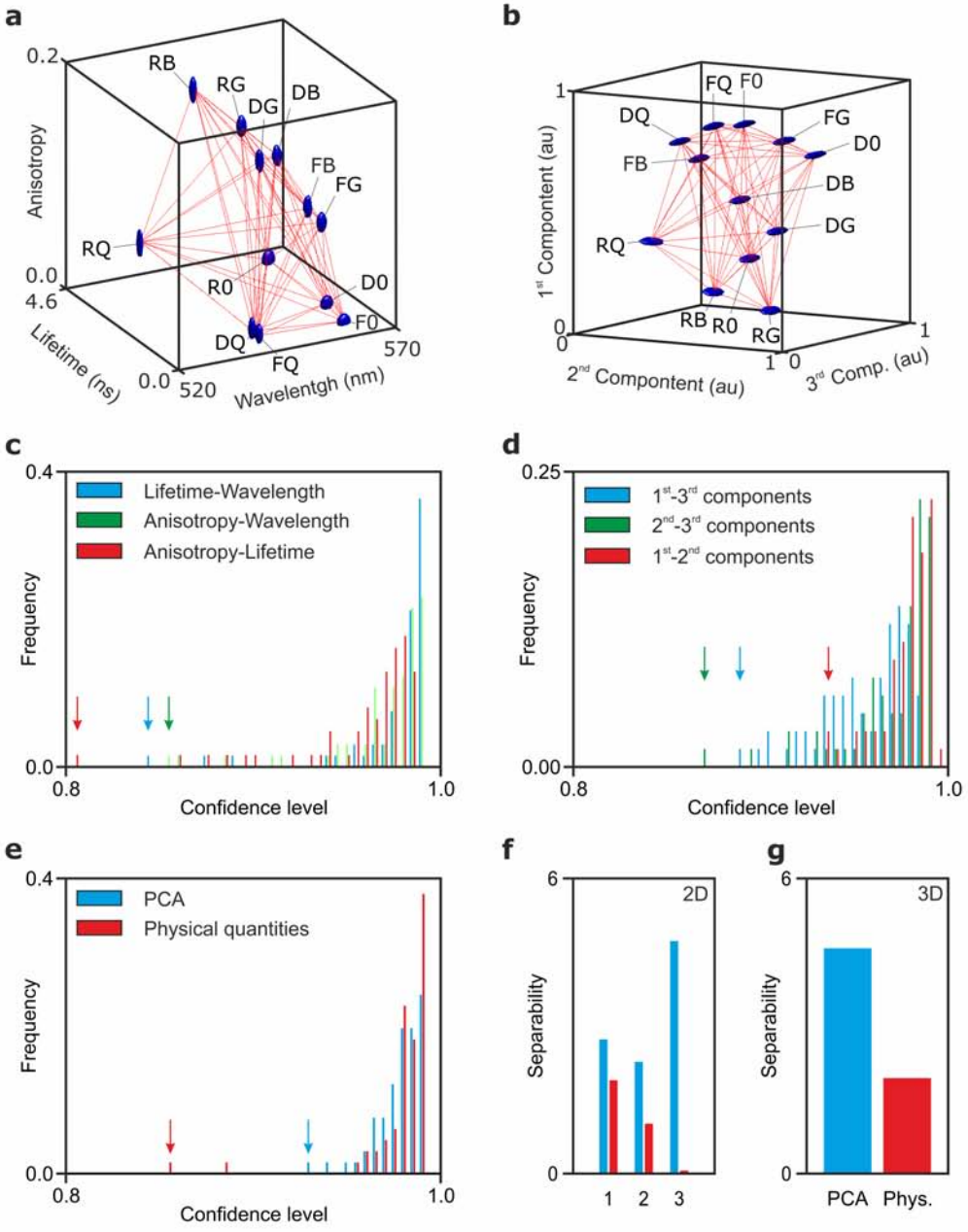
a
0.2
Anisotropy
0.0
4.6
Lifetime (ns)
0.0
520
570
Wavelentgh (nm)
RB
RG
DG
DB
FB
FG
RQ
R0
D0
F0
DQ
FQ
b
1
1st Compontent (au)
0
0
2nd Compontent (au)
1
0
3rd Comp. (au)
1
FQ F0
DQ
FG
D0
FB
DB
DG
RQ
RB R0
RG
c
0.4
Frequency
0.0
0.8
1.0
Confidence level
Lifetime-Wavelength
Anisotropy-Wavelength
Anisotropy-Lifetime
d
0.25
Frequency
0.00
0.8
1.0
Confidence level
1st-3rd components
2nd-3rd components
1st-2nd components
e
0.4
Frequency
0.0
0.8
1.0
Confidence level
PCA
Physical quantities
f
6
Separability
0
1
2
3
2D
g
6
Separability
0
PCA
Phys.
3D

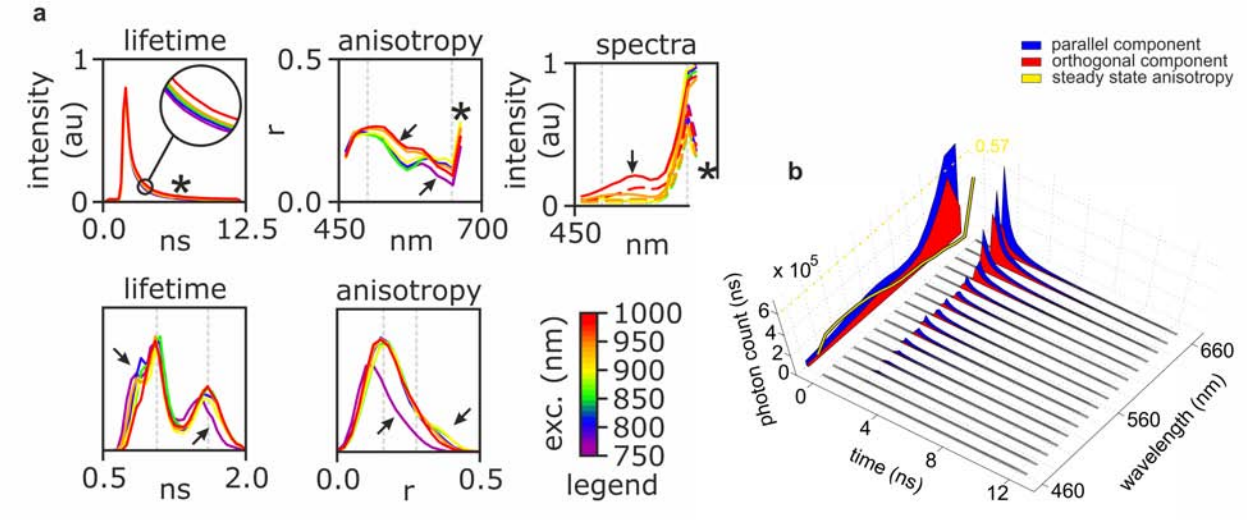

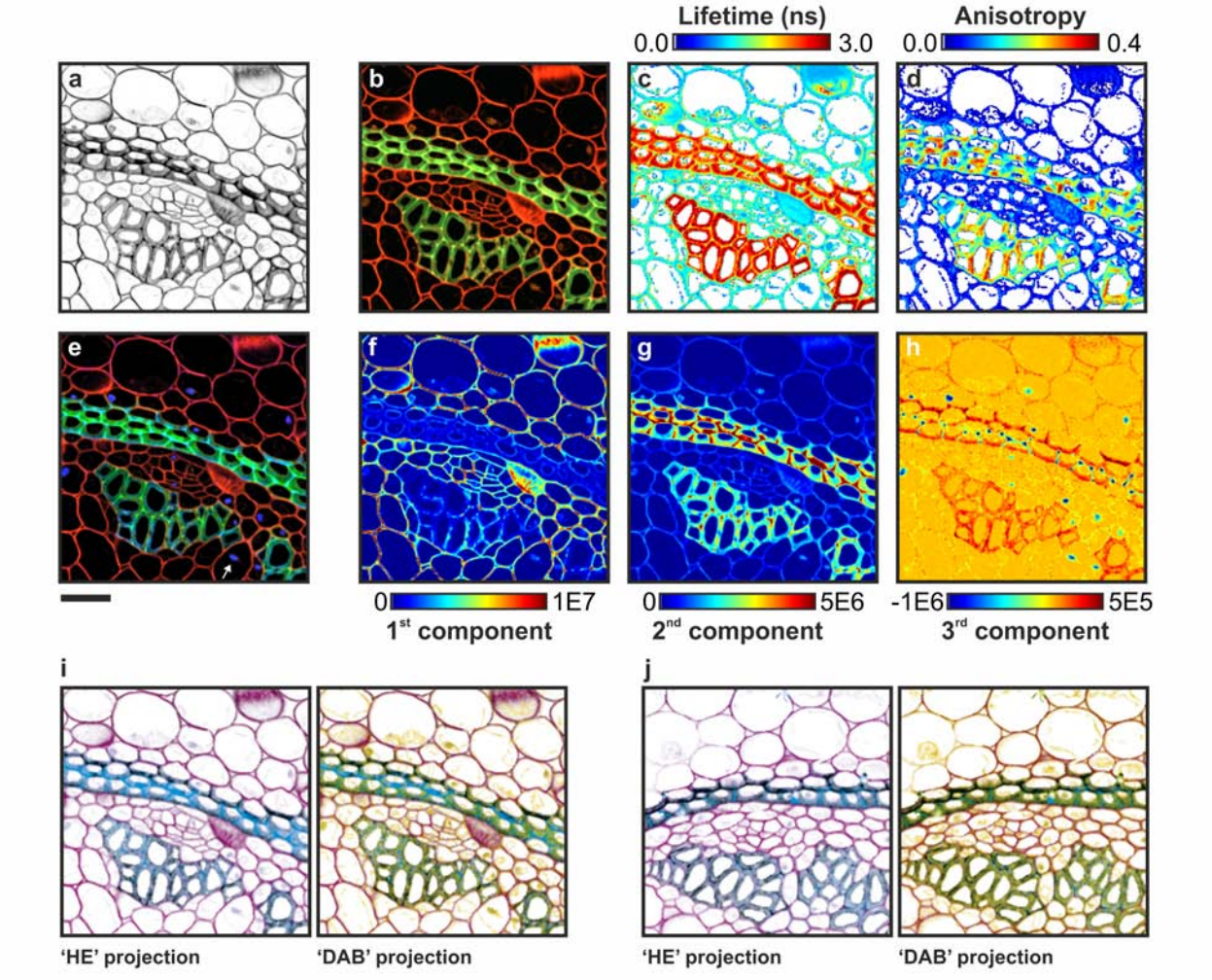
Lifetime (ns)
0.0
3.0
Anisotropy
0.0
0.4
a
b
c
d
e
f
g
h
0
1E7
1st component
0
5E6
2nd component
-1E6
5E5
3rd component
i
j
'HE' projection
'DAB' projection
'HE' projection
'DAB' projection